Revision of manuscript NHESS-2020-135

Dear Editor

We are pleased to submit the revised version of our manuscript on "Semi-empirical prediction of dam height and stability of dams formed by rock slope failures in Norway" following the reviewers' valuable comments.

As mentioned in our replies to both reviewers we added a section on the numerical run-out modelling of rock avalanches, which was used as a validation dataset of our semi-empirical approach. We also followed the suggestion by reviewer #1 to slightly adapt the title of the manuscript. We did, however, not shorten the figure and table captions, because the figures and tables would no longer be self-explanatory without those detailed captions.

We hope that our revised manuscript will be acceptable for publication in NHESS.

With our best regards

Thierry Oppikofer & co-authors

~~Forecasting~~ Semi-empirical prediction of dam height and stability of dams formed by rock slope failures in Norway

Thierry Oppikofer[1], Reginald L. Hermanns[1,2], Vegard U. Jakobsen[2,*], Martina Böhme[1], Pierrick Nicolet[1], Ivanna Penna[1]

[1]Geological Survey of Norway, Leiv Eirikssons vei 39, P.O. Box 6315 Torgarden, 7491 Trondheim, Norway

[2]Norwegian University of Science and Technology, Trondheim, Norway

*Now at: Norwegian Public Roads Administration, Steinskjer, Norway

Correspondence to: Thierry Oppikofer (thierry.oppikofer@ngu.no)

Abstract. Based on an inventory of 69 dams formed by rock slope failures in southwestern Norway and published inventories from other parts of the World we developed semi-empirical relationships linking the maximum dam height ($H_{D.max}$ in m) to dam volume (V_D in 10^6 m³) and other relevant parameters such as valley width (W_V in m) or dam area (A_D in km²). Power-laws are obtained for $H_{D.max} = f(V_D)$ and $H_{D.max} = f(V_D, W_V)$, while a linear relationship links $H_{D.max}$ to the ratio V_D/A_D. For dams in southwestern Norway, the linear relationship $H_{D.max} = 1.75 \times V_D/A_D$ has least uncertainties and provides best results when comparing predicted dam heights with a validation dataset composed of existing dams in northern Norway and numerically modelled dams for possible rock slope failures. To assess the stability of future dams we use the predicted dam heights in the dimensionless blockage index DBI and relating this index to the probability of dam failure derived from our dataset and other published databases on landslide dams. This study underlines the potential of semi-empirical relationships for assessing dam height and stability that needs to be included in preliminary hazard and risk assessment for unstable rock slopes, because damming of a river is an important secondary effect of landslides due to upstream flooding and possible outburst floods in case of dam failure.

1 Introduction

Landslides, and more particularly large rockslides and rock avalanches, have formed natural dams in many mountainous regions (Korup, 2002; Casagli et al., 2003; Evans et al., 2011; Hermanns et al., 2011a; Weidinger, 2011; Dufresne et al., 2018). Even large dams with several millions m³ in volume may be unstable and breach (Hewitt, 1998; Dai et al., 2005; Plaza et al., 2011). Many historic events of landslide dam failures are reported to have occurred within a few days to years after the landslide event, causing catastrophic outburst floods in the valley downstream of the dam (Groeber, 1916; Hewitt, 1982; Costa and Schuster, 1988; Evans, 2006) and leading to major destruction and loss of live (Evans et al., 2011).

The National landslide database of Norway (NVE, 2020) includes at least 181 historical landslides that caused damming of rivers. Most of them were earth and debris slides (153) and only 22 events were rockslides or rock avalanches. Many of those events created only minor damming of rivers without significant consequences. Yet, there were several major events with significant consequences in terms of loss of life or long-lasting landscape changes: the worst natural disaster in Norway's history occurred on 21 September 1345 when the Gaula River was dammed by a massive debris slide that created a 14 km long lake. After only 2–3 days the dam breached leading to a huge outburst flood in the Gaula Valley burying 48 farms and killing at least 500 persons (Furseth, 2006). In 1823, a rock avalanche dammed the Frondøla River and formed the Lintuvatnet Lake (NVE, 2020). The lake is still existing today, even though the dam partially breached leading to an outburst flood in the uninhabited valley. On 26 May 1908, a 1.1 million m³ rock avalanche from the mountain Keipen in the

37   Norang Valley formed a more than 20 m high dam (Figure 1a, b). The impounded lake Lyngstøylvatnet submerged the road

38   and several mountain farms, whose remains are still visible close to the shoreline (Furseth, 2006, Hermanns et al., 2013b).

39   These historic events emphasize the need of addressing the landslide-damming of rivers in landslide risk analyses, including

40   upriver and potential downriver flooding as well as landslide dam stability assessments (Hermanns et al., 2013b). Massive

41   rock slope failures (RSF) may generate tens of meters high dams with long-lasting and potentially catastrophic consequences.

42   The Geological Survey of Norway systematically maps, investigates and analyzes fractured bedrock slopes that might fail

43   catastrophically in the future (Hermanns et al., 2013a). More than 80 unstable rock slopes that during a catastrophic failure

44   will impact and possibly dam rivers have so far been discovered in Norway (NGU, 2020) (Figure 2b). These high numbers

45   set the necessity for cost-effective tools to assess dam heights and dam stability for preliminary risk analyses.

46   The most common tool to assess landslide damming in prospective landslide hazard and risk assessments are likely numerical

47   simulations of the landslide propagation (Hungr, 2011). Examples of such numerical models are the DAN3D code

48   (McDougall and Hungr, 2004; Sosio et al., 2008; Hungr and McDougall, 2009; Schleier et al., 2015, 2016), the Tochnog

49   finite element code (Crosta et al., 2009; Tochnog Professional, 2020) or the RAMMS software suite (Christen et al., 2012).

50   However, these models require numerous input parameters and extensive calibration ~~in order to~~to obtain reliable results,

51   which precludes their cost-efficient use for characterization of ~~a large number of~~many sites, as is required in regional studies.

52   Here we establish semi-empirical relationships for the rapid assessment of the maximum dam height, comparable to those

53   developed for landslide run-out (e.g. Scheidegger, 1973; Corominas, 1996) or landslide-generated displacement waves

54   (Oppikofer et al., 2019). We use an inventory of dams formed by rock slope failures (RSF dams) in southwestern Norway

55   (Figure 2a) along with other published databases on landslide dams (Ermini and Casagli, 2003; Hermanns et al., 2011a;

56   Tacconi Stefanelli et al., 2015) to evaluate the dam height as a function of landslide volume, valley width and dam area. This

57   approach addresses the need for a fast assessment of possible dam formation and stability for potential future RSF, as a part

58   of the systematic hazard and risk analysis of unstable rock slopes in Norway (Hermanns et al., 2012; Oppikofer et al., 2016a,

59   2016b).

60   **2 Methodology**

61   **2.1 Inventory and characteristics of landslide dams**

62   Systematic mapping of RSF dams in southwestern Norway (approximately 120 000 km² in surface) was carried out by

63   Jakobsen (2015) using the online orthophoto map service "Norge i bilder" (Norwegian Mapping Authority, 2020b) and its

64   associated web map service (WMS) in a geographical information system (GIS) (Figure 1b). This aerial photo analysis

65   focused on present-day lakes as an indicator for possible dams, with the aim of identifying lakes that were impounded by

66   RSF. The analysis investigated therefore the immediate downstream surroundings of lakes, looking for deposits, debris and

67   scars of RSF, but also debris from a possible downstream flooding due to a dam breach. It must be noted that dams without

68   remaining lake are therefore not included in present inventory.

69   The detected dams were mapped and registered in a geospatial database, and their geomorphologic characteristics determined

70   based on orthophotos and the national 10-m digital elevation model (DEM) (Norwegian Mapping Authority, 2020a). These

71   dam characteristics include:

72   -   the type of landslide that formed the dam, chiefly rock avalanches (massive RSF with several hundred thousand to

73   millions of cubicmeters in volume and high mobility) and rockslides/rockfalls (RSF with several thousands to hundred

74   thousands of cubicmeters in volume, but without high mobility) or other landslide types;

75   -   the morphologic dam classifications in plan view and in across-valley and along-valley profiles according to Hermanns

76   et al. (2011b) (Figure 3);

77   -   the dam dimensions including valley width W_V, dam width W_D, dam length L_D, dam area A_D, mean dam height $H_{D.mean}$
78   and maximum dam height $H_{D.max}$, dam volume V_D (Figure 4);
79   -   the upstream catchment area A_C and the resulting DBI-value (Ermini and Casagli, 2003);
80   -   an assessment of the dam stability, i.e. whether the dam was unstable and has breached or was (partially) eroded, or was
81   stable and is intact or infilled;
82   -   an assessment of any glacial influence on the dam, especially the initial landslide run-out onto a glacier.

83 The dimensions of the dams were directly mapped in the GIS for valley width W_V, dam width W_D, dam length L_D, dam area
84 A_D (Figure 4a), and the upstream catchment area A_C was calculated using a flow accumulation function in GIS based on the
85 10-m DEM. The mean and maximum dam heights $H_{D.mean}$ and $H_{D.max}$ were estimated based on across-valley and along-valley
86 profiles through the dam (Figure 4b, c). On those profiles, the possible pre-event topography was extrapolated from the
87 surrounding valley morphology, notably the steepness of the valley flanks and the valley width (Figure 4b). In along-valley
88 profiles the morphology prior to the dam was based on a linear interpolation between the beginning of the impounded lake
89 and the foot of the dam (Figure 4c).

90 2.2 Creation of semi-empirical relationships

91 We establish semi-empirical relationships by plotting the maximum dam height relative to various dam characteristics and
92 least-square fitting of functions linking the parameters. The different units of the dam characteristics are accounted for using
93 dimensional analysis. The dam volume V_D, dam area A_D and valley width W_V revealed to be the most relevant dam parameters
94 influencing the maximum dam height $H_{D.max}$, whereas no meaningful correlations were found for other dam characteristics
95 We assess the inherent uncertainties in the obtained relationships by computing the ratio (ρ) between the measured and
96 predicted maximum dam heights. We then fit cumulative frequency distributions of these ratios using lognormal functions
97 to determine the 95th percentile (ρ_{95}). The ratio ρ_{95} yields the upper bound of the 90% prediction interval, meaning that
98 approximately 5% of the measured maximum dam heights exceed the predicted values by a factor of ρ_{95} or more.
99 The dam morphology certainly influences $H_{D.max}$, it is however difficult to predict without detailed modelling studies (see
100 section 2.3), which are beyond the scope of regional studies, for which these semi-empirical relationships are intended.
101 Furthermore, detailed modelling studies most often also include detailed numerical run-out modelling. These run-out models
102 generally provide the thickness of deposits and thus the expected maximum dam height, making the semi-empirical
103 relationships superfluous for detailed local studies.

104 2.3 Numerical run-out modelling of rock slope failures

105 As mentioned in section 2.2, detailed numerical run-out modelling is beyond the scope of regional studies. For this study,
106 however, we used numerical run-out modelling of RSF as validation dataset of our semi-empirical relationships. The
107 Tochnog finite element code was used to model the potential run-out of the unstable rock slope Mannen (Dahle et al., 2011),
108 whereas DAN3D was applied at Ivasnasen, Klingråket, Svarttinden and Gamanjunni (Böhme et al., 2016) (Figure 2b). The
109 reader is referred to above-mentioned publications for complete descriptions of the modelling approach, underlying
110 equations, required input data and parameters.
111 A range of parameters is tested in prospective studies of run-out modelling of RSF: Böhme et al. (2016), for example,
112 modelled the run-out of the Gamanjunni rockslide in DAN3D using a Voellmy rheology for the slide mass with various
113 friction coefficients (ranging between 0.05 and 0.10) and turbulence coefficients (from 500 to 800 ms^{-2}). Depending on the
114 chosen parameters the slide mass spreads differently over the valley bottom giving a range of possible run-out areas and
115 associated thickness of deposits. Plausible models are chosen by expert knowledge and then combined into a final model of
116 the deposits thickness, using for example the maximum of thickness of all retained model runs. The maximum dam height

117     $H_{D.max}$, which is used for comparison with empirically predicted ones, corresponds to the deposits thickness at the location

118   where dam overtopping might occur. That location is computed in a GIS using a *Fill* function based on the computed post-

119   slide DEM.

120   **2.~~43~~ ~~Forecasting~~ Prediction of dam height and stability**

121   The semi-empirical relationships linking $H_{D.max}$ to relevant parameters are used to predict the dam height for future RSF that

122   could dam a river. The dam height $H_{D.max}$ gets added to the elevation of the riverbed to find the possible elevation of the

123   dammed lake. The extent of the impounded lake is obtained by computing the contour line of the lake elevation in the area

124   upstream to the landslide dam.

125   We use the dimensionless blockage index DBI (Ermini and Casagli, 2003) as a proxy to estimate the likelihood of a dam

126   breach. Low DBI-values depict landslide dams that are most likely stable, whereas a high DBI indicates probably unstable

127   dams. We divide the inventory of RSF dams in southwestern Norway and other inventories (Ermini and Casagli, 2003;

128   Hermanns et al., 2011a; Tacconi Stefanelli et al., 2015) into bins of DBI-values containing each 10-12 dams and calculate

129   the proportion of unstable dams for each bin. We then use these proportions to fit a linear function between the lower limit

130   DBI_{lower} below which dams are considered stable, and the upper limit DBI_{upper} above which dams are deemed unstable. In

131   the transition zone between the lower and upper limits, the likelihood of a dam failure p_f increases linearly (Eq. (1)):

132
$$p_f = \begin{cases} 0 & \Leftrightarrow DBI \leq DBI_{lower} \\ \frac{DBI - DBI_{lower}}{DBI_{upper} - DBI_{lower}} & \Leftrightarrow DBI_{lower} < DBI < DBI_{upper} \\ 1 & \Leftrightarrow DBI \geq DBI_{upper} \end{cases} \qquad (1)$$

133   **3 Inventory of landslide dams in southwestern Norway**

134   A total of 69 landslide dams are mapped in southwestern Norway (Figure 2a). Thirty-eight dams were formed by rock

135   avalanches, 29 by rockslides~~/rockfalls~~ and 2 by debris-flows. We discarded those generated by debris-flows from further

136   analyses because the aim of these empirical relationships is to determine the maximum dam height of future RSF.

137   The frequency of rock avalanches in Norway was highest shortly after the last deglaciation, i.e. between 14 000 and 10 000

138   years BP depending on the location (e.g. Böhme et al., 2015; Hermanns et al., 2017). We therefore assume that also most of

139   the RSF dams in southwestern Norway were formed shortly after the retreat of the Scandinavian ice sheet. However, three

140   dams are most likely influenced by glaciers, notably by depositing on decaying glaciers or on dead-ice bodies in the valley.

141   For 10 other dams such a glacial influence is possible. We excluded these 13 dams from further analyses because their

142   dimensions may have been altered by glaciers and are thus not representative for the present-day situation.

143   According to the landform classification by Etzelmüller et al. (2007), most of the 54 remaining dams are in regions with

144   "extreme Alpine relief with over-deepened glacial valleys" or in "high paleic mountain regions with glacial incisions"

145   (Figure 2a). In Rogaland County in southern Norway several clusters of RSF dams are observed in the landform types

146   "glacially scoured low mountains and valleys" and "mountain plateaus" (Figure 2c). These clusters are closely related to

147   WSW-ENE-trending faults (Gabrielsen et al., 2002) forming escarpments that are prone to RSF. Twenty-one dams are intact

148   with a dammed lake and 10 other dams are filled by sediments except a small residual lake. On the side of unstable dams,

149   16 dams are classified as eroded because no deposits of an outburst flood are visible, and 7 dams have failed and likely led

150   to an outburst flood as suggested by related deposits downriver.

151   The morphologic dam classification in plan view according to Hermanns et al. (2011b) reveals that most dams are formed

152   by a RSF completely crossing the valley (Type IIa, n=36) (Figure 3a). Partial damming of the valley by a RSF occurred in

153   5 cases (Type IIc), and 5 dams have multiple lakes (Type IIIa). The across-valley profiles can be classified as symmetrical

154 deposits in a symmetrical valley in 24 cases (Type i), and as asymmetrical with thickest deposits in the distal part in 19 cases

155 (Type ii) (Figure 3b). The classification of the along-valley profiles reveals 21 dams with low thickness and gentle slopes

156 (Type 1) due to the absence of constraints in the valley morphology (Hermanns et al., 2011b), and 29 dams with high

157 thickness and steep slope (Type 2) in a confined valley setting (Figure 3c).

158 Table 1 summarizes the dimensions of the RSF dams in the inventory. The dam length L_D ranges from 45 to 1600 m with a

159 median length of 200 m, whereas the dam width W_D tends to be larger by a factor of 1.7 (median of ratio W_D/L_D) and ranges

160 from 45 to 2800 m with a median width of 330 m. The dam area covers three orders of magnitude with values between

161 5000 m² to 2.7 km² with a median of 53 000 m². The maximum dam heights $H_{D.max}$ vary between 5 and 210 m, whereas the

162 mean dam heights $H_{D.mean}$ vary between 2 and 113 m. The median dam heights are 21 m and 12 m for $H_{D.max}$ and $H_{D.mean}$,

163 respectively. The dam volume V_D computed as the product of A_D and $H_{D.mean}$, spans five orders of magnitude (12 000 m³ to

164 135×10^6 m³). The median dam volume is approximately 1.0×10^6 m³. The cumulative distributions of these dam

165 dimensions can all be fitted by lognormal distributions with very high correlation coefficients ($r^2 > 0.95$ except for W_D)

166 (Table 1).

167 **4 Semi-empirical relationships**

168 We created semi-empirical relationships for the 54 RSF dams in southwestern Norway that were not influenced by glaciers.

169 First, we linked the maximum dam height $H_{D.max}$ (in m) to the dam volume V_D (in 10^6 m³) (Figure 5) by fitting a power-law

170 function (Eq. (2)):

171 $$H_{D.max} = 24.5 \cdot V_D^{1/3} \tag{2}$$

172 The exponent of ⅓ is given by dimensional analysis, whereas the scale factor of 24.5 was fitted with a high correlation

173 coefficient r^2 of 0.73. The ratio ρ between the measured and predicted maximum dam heights ranges from 0.46 to 1.94, and

174 its cumulative frequency distribution can be fitted by a lognormal distribution. The 95th percentile of this distribution

175 ($\rho_{95} = 1.81$) yields the upper bound of the 90% prediction interval of Eq. (2). This implies that approximately 5% of RSF

176 dams in southwestern Norway have a maximum height exceeding the predicted value by 81% or more.

177 Similar power-law functions can be derived from datasets from other studies (Ermini and Casagli, 2003; Hermanns et al.,

178 2011a; Tacconi Stefanelli et al., 2015), with different scale factors, however (Table 2). The scale factor of landslide dams in

179 the Andes (Hermanns et al., 2011a) is much lower than those from other studies (10.1 vs. 21.5 to 24.5). Compared to our

180 inventory, other databases have a larger spread of the data indicated by higher ρ_{95}-values (Table 2).

181 Power-law functions are commonly used in landslide studies to relate the landslide volume to landslide frequency (e.g.

182 Dussauge et al., 2003; Guzzetti et al., 2003), but also other landslide characteristics, such as landslide area (e.g. Hovius,

183 1997). Similarly, the relationship between landslide volume and Fahrböschung, i.e. the ratio between the landslide fall height

184 and travel distance, can be fitted by power-law functions (e.g. Scheidegger, 1973; Nicoletti and Sorriso-Valvo, 1991;

185 Erismann and Abele, 2001; De Blasio, 2011). Furthermore, Oppikofer et al. (2019) found a power-law function linking the

186 run-up height of landslide-generated displacement waves to the landslide volume and distance from impact.

187 Regarding the influence of the morphologic dam classification on the dam height (Table 2), dams classified as asymmetrical

188 with thickest deposits in the distal part (Type ii in across-valley profile) are higher than dams with symmetrical deposits in

189 a symmetrical valley (Type i), but smaller than those partially blocking a valley (Type iv). In along-valley profiles, Type 2

190 dams with high thickness and steep slope are higher than Type 1 dams with low thickness and gentle slopes. Too few data

191 are available for the other dam types in along- or across-valley profiles and in plan view.

192 In narrow valleys the RSF deposits are more confined leading to thicker deposits and thus to a higher dam compared to wide

193 valleys where the deposits are unconfined and spread out over a larger surface. We calculated therefore ratio V_D (in 10^6 m³)

194 over valley width W_V (in m) and fitted following power-law with the exponent given by dimensional analysis (Figure 6, Eq.
195 (3)):

196 $$H_{D.max} = 374 \cdot \left(\frac{V_D}{W_V}\right)^{0.5} \tag{3}$$

197 Ratio ρ between the measured and predicted maximum dam heights ranges from 0.52 to 2.36. The 95th percentile of the
198 lognormal distribution fitted to the cumulative frequency distribution of ρ equals 1.76 (ρ_{95}). This value is slightly smaller
199 than for Eq. (2) ($\rho_{95} = 1.81$). Amongst the other landslide dam inventories, only Tacconi Stefanelli et al. (2015) state W_V.
200 Fitting that dataset with Eq. (3) yields a lower scale factor of 285 and a much higher spread in values testified by lower r²
201 and higher ρ_{95}-values (Figure 6, Table 2).

202 Equation (3) has the expected behaviour with an increase in $H_{D.max}$ for higher volumes and a decrease for wider valleys. The
203 lateral spreading of the landslide deposits in the valley is, however, not accounted for. This could be achieved by including
204 the dam width W_D as additional parameter in a semi-empirical relationship. However, W_D is not independent from V_D and is
205 not easily predictable when using the semi-empirical equations to forecast the dam height for future landslides, except if the
206 run-out area is known. In that case, the dam area A_D (in km²) can be assessed, and the average dam height $H_{D.mean}$ (in m) can
207 be computed as the ratio V_D/A_D as an alternative proxy. For the RSF dams in southwestern Norway, $H_{D.max}$ (in m) increases
208 linearly with $H_{D.mean}$ (Figure 7, Eq. (4)):

209 $$H_{D.max} = 1.75 \cdot H_{D.mean} = 1.75 \cdot V_D/A_D \tag{4}$$

210 The ratio ρ ranges from 0.57 to 1.72 with a value of ρ_{95} of 1.48 (lognormal distribution). This implies that approximately 5%
211 of landslide dams in southwestern Norway have a maximum height exceeding the predicted value by 48% or more. Both the
212 range of ρ and its 95th percentile are significantly smaller than for the other semi-empirical relationships. Again, only the
213 database by Tacconi Stefanelli et al. (2015) contains A_D for few dams. However, we calculated A_D from the published dam
214 width W_D and dam length L_D assuming an elliptic shape of the landslide dam. Using those calculated dam areas in Eq. (4)
215 provides a scale factor of 1.35 (Figure 7, Table 2). Lower r² and higher ρ_{95}-values (0.65 and 1.84, respectively) indicate
216 again a larger spread of the data compared to the inventory of RSF dams in southwestern Norway.

217 **5 Dam stability assessment**

218 Ermini and Casagli (2003) created the DBI as proxy to assess the stability of landslide dams (Eq. (5)):

219 $$DBI = \log_{10}\left(\frac{A_C}{V_D/H_{D.max}}\right) \tag{5}$$

220 With the upstream catchment area A_C in km², the dam volume V_D in 10^6 m³ and the maximum dam height $H_{D.max}$ in m. Ermini
221 and Casagli (2003) found a lower DBI-limit (DBI_{lower}) of 2.75 below which most landslide dams in their inventory are stable,
222 and an upper DBI-limit (DBI_{upper}) of 3.08 above which most dams are unstable. A similar assessment of RSF dams in
223 southwestern Norway (Figure 8a) leads to following observations: (a) one dam with a DBI of 2.33 has failed, but there is
224 also an eroded dam with a DBI of 2.17; (b) there are several stable dams with a DBI > 3.95, yet most dams with a DBI >
225 3.38 have failed or were eroded; (c) the proportion of unstable dams increases with the DBI (Figure 8b) with however a
226 significant drop for high DBI-values in our inventory. Other inventories (Ermini and Casagli, 2003; Hermanns et al., 2011a;
227 Tacconi Stefanelli et al., 2015) show the same tendency with similar proportions of unstable dams for similar bins of DBI-
228 values. Landslide dams in the Andes (Hermanns et al., 2011a) have, however, higher proportions of unstable dams for given
229 DBI-values compared to landslide dams in other regions (Figure 8b). We have therefore not considered the Andean inventory
230 in the joint analysis of dam stability for which we combined the different inventories and divided the dataset again in bins
231 of DBI-values containing 20 dams each (Figure 8c). This histogram can be fitted by a linear regression to obtain
232 $DBI_{lower} = 1.2$ and $DBI_{upper} = 5.0$ used in Eq. (1) to assess the likelihood of a dam failure p_f.

6 Application to predict dam height and stability

6.1 Prediction of maximum dam height

We use the semi-empirical relationships (Eq. (2), (3) and (4)) to predict the maximum dam height generated by a future rock slope failure damming a valley. We thereby use following assumptions and methods:

- The dam volume V_D is equal to the slide volume V_S times a bulking factor of 1.25 (25% volume increase due to fracturing of the rock mass and porosity of the deposits) (Hungr and Evans, 2004). This implies that the entire volume reaches the valley and forms the dam. This is obviously the worst-case scenario as shown by Ermini and Casagli (2003) with an average ratio V_D/V_S of 40% for rainfall-triggered landslides and 57% for earthquake-triggered landslides. In Norway, however, numerical run-out modelling for the six unstable rock slopes used for the validation of the semi-empirical relationships (see Table 3) shows that in general ca. 90% of V_S reach the valley bottom to form a dam.
- The valley width W_V used in Eq. (3) is measured on a cross-section along the centre line of the run-out area and roughly perpendicular to the valley axis restricted to the flat valley bottom, i.e. slope angles smaller than 10°;
- The dam area A_D used in Eq. (4) is assessed iteratively based on the run-out area, which can be assessed using simple modelling tools, such as the Fahrböschung or angle of reach (Scheidegger, 1973; Corominas, 1996) implemented in the software CONEFALL (Jaboyedoff and Labiouse, 2011) or the software Flow-R (Horton et al., 2013, Oppikofer et al., 2016a, 2016b) (Figure 9): (a) as first approximation of A_D we use the run-out area in the flat valley bottom to compute $H_{D.max}$; (b) we then clip the run-out area to this first approximation of the dam elevation (elevation of the valley floor plus $H_{D.max}$) to obtain a new approximation of A_D, which in turn is used in Eq. (4) for a new estimation of $H_{D.max}$; (c) this procedure is repeated until the difference between successive estimations of $H_{D.max}$ is smaller than a threshold of 1 m.

The area of the impounded lake corresponds to the contour line of the estimated dam elevation (elevation of the valley floor plus $H_{D.max}$) (Figure 9a).

6.2 Prediction of dam stability

The maximum dam height $H_{D.max}$ predicted by the semi-empirical relationships can then be used to assess the dam stability using the DBI (Ermini and Casagli, 2003) (Eq. (5)). The catchment area A_C upstream of the dam can be easily assessed with a "flow accumulation" GIS-function provided that the DEM covers the entire upstream catchment area. The resulting DBI-values are in turn used in Eq. (1) to assess the probability of failure p_f.

6.3 Validation of semi-empirical relationships

To test the semi-empirical relationships for RSF dams in southwestern Norway, we analyzed four RSF dams in northern Norway as validation dataset. Those dams are presently stable or infilled (Fig. 2b). In addition, the relationships were validated by comparing predicted dam heights with results from detailed numerical run-out modelling for six unstable rock slopes (see Böhme et al., 2016 for an example; NGU, 2020).

Table 3 shows the measured or modelled dam characteristics (V_D, W_V, A_D, A_C, $H_{D.max}$) and the predicted maximum dam heights $H_{D.max}$ using the semi-empirical relationships in Eq. (2), (3) and (4). This comparison shows that Eq. (4) provides the best match with measured/modelled dam heights in 8/10 cases, whereof all six potential future rock slope failures. For Eq. (4) the average relative error is ±13%, which is very small considering the relatively large uncertainties on the semi-empirical relationship itself with a ρ_{95} of 1.48 (see above). For Eq. (2) and (3) the average relative errors are also acceptable when considering only the four existing RSF dams in northern Norway (±29% and ±20%, respectively). Regarding the six future RSF dams however, the average relative errors become inacceptable (±267% and ±202%, respectively). Possible reasons for this huge discrepancy are discussed below. Based on this validation dataset we consider Eq. (4) as best possible semi-empirical relationship to predict the maximum dam height $H_{D.max}$.

7 Discussion

7.1 Differences between landslide dam inventories

The inventory of landslide dams in southwestern Norway and other inventories used in this study (Ermini and Casagli, 2003; Hermanns et al., 2011a; Tacconi Stefanelli et al., 2015) contain significant differences, notably the landslide processes considered, the geological settings and the volume estimations.

Our inventory of landslide dams in SW Norway and the Andean inventory by Hermanns et al. (2011a) focus on rock slope failures (rock avalanches and rock falls) and not on other landslide processes (two dams generated by debris-flows were discarded from analyses). Conversely, the worldwide inventory of Ermini and Casagli (2003) and the Italian dataset by Tacconi Stefanelli et al. (2015) contain various landslide types (rock avalanches, rock falls, debris flows, translational and rotation slides etc.). Based on the published information, it is unfortunately impossible to extract only dams generated by rock slope failures from those inventories. Yet, such a separation into landslide types would likely improve to comparability between the different inventories and the ensuing differences related to the geological settings.

The relationship between the maximum dam height and dam volume (Figure 5) shows a wide spread in values, i.e. a RSF dam with a volume of 1×10^6 m³ can lead to a dam height ranging from 4 to 55 m. However, there is no significant difference between our inventory and the datasets by Ermini and Casagli (2003) and Tacconi Stefanelli et al. (2015), which is reflected in the power-law distributions fitted to the different inventories (Table 2). The Andean inventory (Hermanns et al., 2011a) shows, however, significantly lower dam heights for a given volume compared to the other datasets (Figure 5, Table 2). This is related to the different geomorphic/tectonic settings of the Andean inventory with often tens of kilometer wide valleys, compared to more Alpine settings used in our and other inventories.

Finally, the assessment of the dam volume is a crucial parameter for all semi-empirical relationships established in this study. The approach chosen here follows the method by Hermanns et al. (2011a), i.e. the extrapolation of the topography prior to the landslide dam formation using across-valley and along-valley profiles (Figure 4b, c) to assess $H_{D.mean}$ and $H_{D.max}$. Multiplying the $H_{D.mean}$ with the dam area A_D yields the dam volume V_D. The method used to estimate V_D. is not specified for the other inventories (Ermini and Casagli, 2003, Tacconi Stefanelli et al., 2015) as they are collections of several other datasets. In the inventory by Tacconi Stefanelli et al. (2015) many volumes appear to be computed as the product of dam width, dam length and dam height (in 11% of the cases or as the same product divided by a factor of 2 (in 35% of the cases). This emphasizes the uncertainties linked to the volume estimates. A thorough reanalysis of the different landslide dam inventories using a common approach would likely improve the reliability of the semi-empirical relationships proposed in this study. A promising technique to assess the volume of landslide deposits is the Sloping Local Base Level technique (Jaboyedoff et al., 2004, 2020) that uses a digital elevation model and the extent of the landslide deposits to compute the possible pre-landslide topography. Jaboyedoff et al. (2020) review different techniques that can be useful to assess volumes of landslides and their deposits.

7.2 Dam stability assessment

The dimensionless blockage index DBI (Ermini and Casagli, 2003) is widely accepted in the assessment of landslide dam stability (e.g. Tacconi Stefanelli et al., 2016, 2018; Dufresne et al., 2018). Other geomorphic analyses were proposed (e.g. Korup, 2004, Dong et al., 2009), but the extraction of the required parameters is more laborious and often even not feasible for paleo dams, or the approach was only tested on a local inventory.

The DBI-values for landslide dams in southwestern Norway cover a similar range than those from other inventories (Figure 8). It is however surprising to have several stable landslide dams with DBI-values significantly higher than the "unstable limits" defined in other studies, i.e. 3.08 in Ermini and Casagli (2003) or 3.57 in Tacconi Stefanelli et al. (2015). Our inventory contains 16 landslide dams with a DBI > 3.57, whereof only 8 were eroded or breached and 8 are still intact. The

proportion of unstable dams in the bin with highest DBI-values is indeed significantly lower (4 unstable dams out of 10 dams) than in the bin with second-highest DBI-values (9 out of 11) (Figure 8b). Possible reasons for this difference with other inventories are:

- In the creation of our inventory, we focused on existing lakes impounded by landslide deposits as identification criteria. Landslide dams without remaining lake are thus not included, yet many of those dams were likely unstable. Extending the inventory to all RSF dams might thus increase the overall proportion of unstable dams (23 out of 54), especially also for higher DBI-values.

- Most dams in our inventory formed in prehistoric times and the stability assessment of these paleo dams is solely based on geomorphologic observations. In other datasets (Ermini and Casagli, 2003, Tacconi Stefanelli et al., 2015) most landslide events occurred in historic times and available historical records help distinguishing between intact, eroded and breached dams.

- The RSF deposits impounding the lakes in southwestern Norway often have a large grain size (Figure 1c, e, f). Grain size analysis of RSF dams shows a median diameter of 0.6 to 0.9 m, and boulders of more than 2 m in diameter form up to 15% of the deposits (Jakobsen, 2016). In comparison, Casagli et al. (2003) obtained median grain sizes ranging from 0.0044 mm to 0.32 m for landslide dams in the Northern Apennines. The large grain size of RSF dams in southwestern Norway could explain the relatively higher stability compared to (possibly) finer grained deposits in other parts of the World. Deposits with larger grain size are more resistant to erosion and favor drainage through the rock avalanche deposits (Casagli et al., 2003; Dunning, 2006; Weidinger, 2011) (Figure 1c).

Using the proportion of unstable dams in bins of DBI-values for the combined inventory (Ermini and Casagli, 2003, Tacconi Stefanelli et al., 2015 and our dataset) yields a much broader range for the transition zone between the "stable domain" and "unstable domain" than in previous studies (Figure 8). This reanalysis of the joint dataset is robust as it considers possible outliers and it is less dependent on single values. One could for example argue to set the upper limit DBI_{upper} to the highest DBI-value of all stable dams (4.37 instead of 5.0). This would imply that DBI_{upper} is solely depending on a single landslide dam, which is not appropriate given the complexity of the phenomena and the uncertainties in the inventories. We did not include the dataset by Hermanns et al. (2011a) into the combined inventory due to the significantly higher proportion of unstable dams for given DBI-classes (Figure 8a, b). A possible reason is the relatively lower dam heights in the Andes compared to other datasets (see discussion above), which leads to lower DBI-values. Other causes for this difference could be the grain size of deposits, climatic conditions and the age of the Andean dams, which are up to 60 ka old (Hermanns et al., 2004, 2011a, Costa and González Díaz, 2007)

It would be interesting to perform this stability assessment for different geological, geomorphological and climatic environments, in order to obtain lower and upper DBI-limits for different conditions. This requires however more complete inventories, as at least 100 or 150 landslide dams are required to obtain a sufficient number of bins (10 to 15 bins) containing each a sufficient number of dams ($\geq$10).

7.3 Prediction of dam height using semi-empirical relations or numerical modelling

Two of the proposed semi-empirical relationships rely only on the dam volume V_D (Eq. (2)), or on the ratio V_D over valley width W_V (Eq. (3)). These equations are thus a quick tool to assess the dam height, yet comparison with numerical modelling shows that these relationships overestimate the maximum dam height (Table 3). The third proposed semi-empirical relationship using the ratio V_D over dam area A_D (Eq. (4)) provides a better match with numerical modelling results, requires however a simple run-out analysis to assess the run-out area and estimate A_D (Figure 9). A first assessment of the landslide run-out area can be achieved by calculating the landslide run-out length L as a function of the landslide fall height H and the volume-dependent angle of reach α (e.g. Scheidegger, 1973; Nicoletti and Sorriso-Valvo, 1991; Erismann and Abele, 2001; De Blasio, 2011) (Figure 4b). The angle of reach α is also used in more advanced computer programs, such as CONEFALL

356 (Jaboyedoff and Labiouse, 2011) or Flow-R (Horton et al., 2013), which require little to no calibration and can thus be

357 quickly applied to assess the run-out area. Yet, these tools do not provide the thickness of deposits and thus the dam height.

358 The third semi-empirical relationship $H_{D.max} = f(V_D/A_D)$ (Eq. (4)) yields the maximum dam height based on the landslide run-

359 out area and dam area.

360 Using detailed numerical simulations of the landslide propagation and run-out, such the DAN3D code (McDougall and

361 Hungr, 2004) or the RAMMS software suite (Christen et al., 2012), directly provide the thickness of landslide deposits and

362 allows to find the lowest elevation of the post-slide topography up to which a lake can form (see Oppikofer et al., 2016a,

363 Figure 9). However, these simulations require many input parameters and extensive calibration in order to obtain reliable

364 results. These requirements impede their cost-efficient use in regional studies, where a large number of potential landslide

365 dams need to be assessed.

366 The proposed semi-empirical relationships are a conservative method because they assess the maximum dam height and thus

367 not the lowest elevation where dam overtopping may occur. Numerical simulations on the other hand provide the dam height

368 and elevation where overtopping would occur. This difference partly explains the discrepancy between numerically modelled

369 and empirically predicted dam heights (Table 3). Another possible reason for this discrepancy is the difference between

370 observed and modelled run-out areas. The effective run-out area of a landslide can be significantly smaller than numerically

371 simulated ones: the latter generally cover the entire area potentially affected by a landslide, while the real run-out area of a

372 landslide event may only cover parts of the total area. As the landslide volume in reality may spread over a smaller area than

373 simulated, the average and maximum dam heights obtained by numerical simulations or by Eq. (4) may be too small. Yet,

374 the possible overestimation of A_D is counterbalanced by conservative estimate of V_D being the entire landslide volume V_S

375 times a bulking factor of 1.25. More back-analyses of landslide-generated dams are required to ascertain these possible

376 differences between modelled and real run-out areas. In turn, this could lead to an improved workflow for assessing the dam

377 height and reducing uncertainties.

378 These considerations highlight the necessity to assess uncertainties on dam height and stability by using various approaches,

379 including different semi-empirical relationships, but also numerical simulations for critical areas. To assess uncertainties,

380 we calculate for example the DBI and p_f using $H_{D.max}$ for the potential RSF dams of the validation dataset (see Table 3).

381 Compared to the results from numerical simulations, the DBI increases in average by 0.64 and 0.56 for Eq. (2) and (3),

382 respectively. This leads in turn to an average increase of p_f of +16% and +14%, respectively. This comparison highlights

383 that despite large uncertainties, the influence on dam stability and thus on the consequences assessment is relatively

384 moderate.

385 **8 Conclusions & perspectives**

386 The semi-empirical relations presented here provide a rapid approach for predicting the maximum dam height of dams that

387 might result from the future failure of an unstable rock slope. All relations require only limited input parameters, chiefly the

388 slide volume, the valley width and the dam area based on simple run-out assessments. These semi-empirical relationships

389 are established from an inventory of 54 RSF dams in southwestern Norway with dam volumes ranging from 12 000 m³ to

390 135×10^6 m³. Only dams generated by catastrophic rockslides or rock avalanches and without any glacial influence were

391 included in the analyses. Consequently, the semi-empirical relations presented here may be less or not applicable for other

392 landslide types (e.g. debris-flows, shallow landslides) and other volume classes. The upper bounds of the 90% prediction

393 intervals of these semi-empirical relationships range from 1.48 to 1.81, meaning that approximately 5% of the actual

394 maximum dam heights exceed the predicted value by 48% to 81% or more.

395 Validation of the semi-empirical relationships was performed using four RSF dams in northern Norway, but also results

396 from detailed numerical run-out simulations for six unstable rock slopes. The maximum dam heights predicted by the semi-

397 empirical relations are generally in good agreement with the measured/modelled dam heights from the validation dataset.

398 Best validation results are obtained for the relationship linking maximum dam height to landslide volume and dam area with

399 only a modest overestimation of the maximum dam heights (average relative error of 18%). This semi-empirical relationship

400 provides thus an appropriate tool for the first-order assessment of dams generated by rock slope failures at a local to regional

401 scale. Using limited input parameters, this relationship allows the prediction of the maximum dam height and thus the

402 upstream inundation area, but also to quickly forecast the dam stability using the dimensionless blockage index.

403 Possible improvements of these semi-empirical relationships are the inclusion of additional datasets, notably existing

404 landslide dams from other regions in Norway. Similar datasets could be collected for other mountainous regions in the

405 World, possibly leading to semi-empirical relationships with different parameters than those presented here for dams from

406 rock slope failures in southwestern Norway. Another possible major improvement consists in the addition of those dams that

407 do not possess a lake or residual lake at present. This requires however very time-intensive screening over large regions to

408 detect the landslide deposits that might have blocked a river in the past. Furthermore, the presented semi-empirical

409 relationships are only valid for rockslides and rock avalanches. Similar semi-empirical relationships can be imagined for

410 other landslide types, but more complete datasets on those landslide dams are required first. We strongly suggest using the

411 predictive tools developed here to assess landslide dam formation and stability, which should be an integral part of risk

412 assessment for future landslide events.

413 **Data availability**

414 Data used for this study are available on DataverseNO: Oppikofer, T., Hermanns, R.L., Jakobsen, V.U., Böhme, M., Nicolet,

415 P., Penna, I.: Database on landslide dams in southwestern Norway, DataverseNO, https://doi.org/10.18710/47DXWT, 2020.

416 **Author contribution**

417 RH and TO conceptualized and supervised the study; VJ created the landslide dam inventory; TO analysed the study data

418 with support from MB, PN, IP and RH; TO prepared the manuscript with contributions from all co-authors.

419 **Competing interests**

420 The authors declared that they do not have any competing interests.

421 **Acknowledgements**

422 We are grateful to the Norwegian Water Resources and Energy Directorate for funding this project through the national

423 mapping program for unstable rock slopes in Norway.

424 **References**

425 Böhme, M., Oppikofer, T., Longva, O., Jaboyedoff, M., Hermanns, R.L., and Derron, M.-H.: Analyses of past and present

426 rock slope instabilities in a fjord valley: implications for hazard assessment. Geomorphology, 248, 464–474,

427 https://doi.org/10.1016/j.geomorph.2015.06.045, 2015.

428 Böhme, M., Bunkholt, H., Dehls, J.F., Oppikofer, T., Hermanns, R.L., Dalsegg, E., Kristensen, L., Lauknes, T.R., and

429 Eriksen, H.Ø.: Geologisk modell og fare- og risikoklassifisering av det ustabile fjellpartiet Gamanjunni 3 i Manndalen,

430 Troms. Geol. Surv. Norw., Trondheim, Norway, NGU report 2016.031, 63 pp., 2016 (in Norwegian).

Casagli, N., Ermini, L., and Rosati, G.: Determining grain size distribution of the material composing landslide dams in the Northern Apennines: sampling and processing methods. Eng. Geol., 69, 83–97, https://doi.org/10.1016/S0013-7952(02)00249-1, 2003.

Christen, M., Bühler, Y., Bartelt, P., Leine, R., Glover, J., Schweizer, A., Graf, C., McArdell, B.W., Gerber, W., Deubelbeiss, Y., Feistl, T., and Volkwein, A.: Integral hazard management using a unified software environment: numerical simulation tool "RAMMS" for gravitational natural hazards, in: Proceedings of the 12th Congress INTERPRAEVENT, Grenoble, France, 23-26 April 2012, 77–86, 2012.

Corominas, J.: The angle of reach as a mobility index for small and large landslides. Can. Geotech. J., 33, 260–271, 1996.

Costa, C.H. and González Día, E.F.: Age constraints and paleoseismic implication of rock avalanches in the northern Patagonian Andes, Argentina. J. S. Am. Earth Sci., 24, 48–57, 2007.

Costa, J.E. and Schuster, R.L.: The formation and failure of natural dams. Bull. Geol. Soc. Am., 100, 1054–1068, https://doi.org/10.1130/0016-7606(1988)100%3C1054:TFAFON%3E2.3.CO;2, 1988.

Crosta, G.B., Imposimato, S., and Roddeman, D.: Numerical modelling of entrainment/deposition in rock and debris-avalanches. Engineering Geology, 109, 135-145, https://doi.org/10.1016/j.enggeo.2008.10.004, 2009.

Dai, F.C., Lee, C.F., Deng, J.H., and Tham, L.G.: The 1786 earthquake-triggered landslide dam and subsequent dam-break flood on the Dadu River, southwestern China. Geomorphology, 65, 205–221, https://doi.org/10.1016/j.geomorph.2004.08.011, 2005.

Dahle, H., Bjerke, P.L., Crosta, G.B., Hermanns, R.L., Anda, E., and Saintot, A.: Faresoner for utløp, oppdemming og flom som følge av fjellskredfare ved Mannen. Geol. Surv. Norw., Trondheim, Norway, NGU report 2011.058, 41 pp., 2011 (in Norwegian).

De Blasio, F.V.: Introduction to the physics of landslides. Springer Science & Business Media, 2011.

Dong, J.J., Tung, Y.H., Chen, C.C., Liao, J.J., and Pan, Y.W.: Discriminant analysis of the geomorphic characteristics and stability of landslide dams. Geomorphology, 110, 162–171, https://doi.org/10.1016/j.geomorph.2009.04.004, 2009.

Dufresne, A., Ostermann, M., and Preusser, F.: River-damming, late-Quaternary rockslides in the Ötz Valley region (Tyrol, Austria). Geomorphology, 310,153–167, 2018.

Dunning, S.A.: The grain size distribution of rock-avalanche deposits in valley confined settings. Italian Journal of Engineering Geology and Environment, Special issue 1, 117–121, https://doi.org/10.4408/IJEGE.2006-01.S-15, 2006.

Dussauge, C., Grasso, J.-R., and Helmstetter, A.: Statistical analysis of rockfall volume distributions: Implications for rockfall dynamics. J. Geophys. Res. (Solid Earth), 108(B6), 2286, https://doi.org/10.1029/2001JB000650, 2003

Erismann, T.H. and Abele, G.: Dynamics of rockslides and rockfalls. Springer, Berlin, 2001.

Ermini, L. and Casagli, N.: Prediction of the behaviour of landslide dams using a geomorphological dimensionless index. Earth Surf. Proc. Land. 28, 31–47, 2003.

Etzelmüller, B., Romstad, B., and Fjellanger, J.: Automatic regional classification of topography in Norway. Norw. J. Geol. 87, 167–180, 2007.

Evans, S.G.: The formation and failure of landslide dams: an approach to risk assessment. Italian Journal of Engineering Geology and Environment, Special issue 1, 15–20, https://doi.org/10.4408/IJEGE.2006-01.S-02, 2006.

Evans, S.G., Delaney, K.B., Hermanns, R.L., Strom, A., and Scarascia-Mugnozza, G.: The formation and behaviour of natural and artificial rockslide dams; implications for engineering performance and hazard management, in: Natural and Artificial Rockslide Dams, edited by: Evans, S.G., Hermanns, R.L., Strom, A., Scarascia-Mugnozza, G., Lecture Notes in Earth Sciences, vol. 133, Springer, Berlin, Heidelberg, Germany, pp 1–75, 2011.

Furseth, A.: Skredulykker i Norge. Tun Forlag, Oslo, Norway, 2006 (in Norwegian).

Gabrielsen, R.H,, Braathen, A., Dehls, J., and Roberts, D.: Tectonic lineaments of Norway. Norw. J. Geol., 82, 153–174, 2002.

474 Groeber, P.: Informe sobre las causas que han producido las crecientes del río Colorado (Territorios del Neuquén y La
475 Pampa) en 1914. Ministerio de Agricultura de la Nacíon (Argentina), Dirección General de Minas, Buenos Aires. Geología
476 e Hidrogeología, Serie B (Geología), Bull 11, 1–29, 1916.

477 Guzzetti, F., Reichenbach, P., and Wieczorek, G.F.: Rockfall hazard and risk assessment in the Yosemite Valley, California,
478 USA. Nat. Haz. Earth Syst. Sci., 3, 491–503, 2003.

479 Hermanns, R.L., Niedermann, S., Ivy-Ochs, S., and Kubik, P.: Rock avalanching into a landslide-dammed lake causing
480 multiple dam failure in Las Conchas valley (NW Argentina) – evidence from surface exposure dating and stratigraphic
481 analyses. Landslides, 1, 113–122, 2004.

482 Hermanns, R.L., Folguera, A., Penna, I., Fauqué, L., and Niedermann, S.: Landslide Dams in the Central Andes of Argentina
483 (Northern Patagonia and the Argentine Northwest), in: Natural and Artificial Rockslide Dams, edited by: Evans, S.G.,
484 Hermanns, R.L., Strom, A., Scarascia-Mugnozza, G., Lecture Notes in Earth Sciences, vol. 133, Springer, Berlin,
485 Heidelberg, Germany, pp 147–176, 2011a.

486 Hermanns, R.L., Hewitt, K., Strom, A., Evans, S.G., Dunning, S.A., Scarascia-Mugnozza, G.: The Classification of
487 Rockslide Dams, in: Natural and Artificial Rockslide Dams, edited by: Evans, S.G., Hermanns, R.L., Strom, A., Scarascia-
488 Mugnozza, G., Lecture Notes in Earth Sciences, vol. 133, Springer, Berlin, Heidelberg, Germany, pp 581–593, 2011b.

489 Hermanns, R.L., Oppikofer, T., Anda, E., Blikra, L.H., Böhme, M., Bunkholt, H., Crosta, G.B., Dahle, H., Devoli, G.,
490 Fischer, L., Jaboyedoff, M., Loew, S., Sætre, S., and Yugsi Molina, F.X.: Recommended hazard and risk classification
491 system for large unstable rock slopes in Norway, Geol. Surv. Norw., Trondheim, Norway, NGU report 2012.029, 52 pp.,
492 2012.

493 Hermanns, R.L., Blikra, L.H., Anda, E., Saintot, A., Dahle, H., Oppikofer, T., Fischer, L., Bunkholt, H., Böhme, M., Dehls,
494 J.F., Lauknes, T.R., Redfield, T.F., Osmundsen, P.T., and Eiken, T.: Systematic Mapping of Large Unstable Rock Slopes in
495 Norway, in: Landslide Science and Practice, vol. 1, edited by: Margottini, C., Canuti, P., and Sassa, K., Springer, Berlin,
496 Heidelberg, Germany, 29–34, 2013a.

497 Hermanns, R.L., Dahle, H., Bjerke, P.L., Crosta, G.B., Anda, E., Blikra, L.H., Saintot, A., and Longva, O.: Rockslide Dams
498 in Møre og Romsdal County, Norway, in: Landslide Science and Practice, vol. 6, edited by: Margottini, C., Canuti, P., and
499 Sassa, K., Springer, Berlin, Heidelberg, Germany, 3–12, 2013b.

500 Hermanns, R.L., Schleier, M., Böhme, M., Blikra, L.H., Gosse, J.C., Ivy-Ochs, S., Hilger, P.: Rock-Avalanche Activity in
501 W and S Norway Peaks After the Retreat of the Scandinavian Ice Sheet, in: WLF 2017: Advancing Culture of Living with
502 Landslides, edited by: Mikoš, M., Vilímek, V., Yin, Y., Sassa, K., Springer, Cham, Switzerland, 331–338, 2017.

503 Hewitt, K.: Natural Dams and Outburst Floods in the Karakoram Himalaya, in: Hydrological Aspects of Alpine and High
504 Mountain Areas (Proceedings of the Exeter Symposium, July 1982), vol 138, International Association of Hydrological
505 Sciences, Wallingford, UK, 259–269, 1982.

506 Hewitt, K.: Catastrophic landslides and their effects on the Upper Indus streams, Karakoram Himalaya, northern Pakistan.
507 Geomorphology, 26, 47–80, 1998.

508 Horton, P., Jaboyedoff, M., Rudaz, B., Zimmermann, M.: Flow-R, a model for susceptibility mapping of debris flows and
509 other gravitational hazards at a regional scale. Nat. Haz. Earth Syst. Sci., 13, 869–885, https://doi.org/10.5194/nhess-13-
510 869-2013, 2013.

511 Hovius, N.: Sediment flux from a mountain belt derived by landslide mapping. Geology, 25, 231–234, 1997.

512 Hungr, O.: Prospects for Prediction of Landslide Dam Geometry Using Empirical and Dynamic Models, in: Natural and
513 Artificial Rockslide Dams, edited by: Evans, S.G., Hermanns, R.L., Strom, A., Scarascia-Mugnozza, G., Lecture Notes in
514 Earth Sciences, vol. 133, Springer, Berlin, Heidelberg, Germany, 463–477, 2011.

515 Hungr, O and Evans, S.G.: Entrainment of debris in rock avalanches: An analysis of a long run-out mechanism. Geol. Soc.
516 Am. Bull., 116, 1240–1252, https://doi.org/10.1130/B25362.1, 2004.

Hungr, O., and McDougall, S.: Two numerical models for landslide dynamic analysis. Computers & Geosciences, 35, 978–992, https://doi.org/10.1016/j.cageo.2007.12.003, 2009.

Jaboyedoff, M. and Labiouse, V.: Technical Note: Preliminary estimation of rockfall runout zones. Nat. Haz. Earth Syst. Sci., 11, 819–828, https://doi.org/10.5194/nhess-11-819-2011, 2011.

Jaboyedoff, M., Baillifard, F., Couture, R., Locat, J., and Locat, P.: Toward preliminary hazard assessment using DEM topographic analysis and simple mechanical modeling by means of sloping local base level, in: Landslides: Evaluation and Stabilization, edited by: Lacerda, W.A., Ehrlich, M., Fontoura, A.B., and Sayão, A., Taylor & Francis Group, London, 199–205, 2004.

Jaboyedoff, M., Carrea, D., Derron, M.-H., Oppikofer, T., Penna, I.M., and Rudaz, B.: A review of methods used to estimate initial landslide failure surface depths and volumes. Eng. Geol., in press, https://doi.org/10.1016/j.enggeo.2020.105478, 2020.

Jakobsen, V.U.: Investigation of rockslide dams in the southwestern part of Norway. Project thesis, Norwegian University of Science and Technology, Trondheim, Norway, 2015.

Jakobsen, V.U.: An empirical approach for determining the evolution and behavior of rockslide dams. MSc thesis, Norwegian University of Science and Technology, Trondheim, Norway, 2016.

Korup, O.: Recent research on landslide dams; a literature review with special attention to New Zealand. Prog. Phys. Geog., 26, 206–235, https://doi.org/10.1191/0309133302pp333ra, 2002.

Korup, O.: Geomorphometric characteristics of New Zealand landslide dams. Eng. Geol., 73,13–35, 2004.

McDougall, S. and Hungr, O.: A model for the analysis of rapid landslide motion across three-dimensional terrain. Can. Geotech. J., 41, 1084–1097, https://doi.org/10.1139/T04-052, 2004.

NGU: Unstable Rock Slopes – National Database for Unstable Rock Slopes. http://geo.ngu.no/kart/ustabilefjellparti_mobil/, last access: 23 September April 2020.

Nicoletti, G. and Sorriso-Valvo, M.: Geomorphic controls of the shape and mobility of rock avalanches. Geol. Soc. Am. Bull., 103, 1365–1373, 1991.

Norwegian Mapping Authority: Height DTM 10 – Map Catalogue. https://kartkatalog.geonorge.no/metadata/dddbb667-1303-4ac5-8640-7ec04c0e3918, last access: 23 September April 2020, 2020a.

Norwegian Mapping Authority: Norge i bilder – Online map service for orthophotos. https://www.norgeibilder.no/, last access: 23 April September 2020, 2020b.

NVE: Skredatlas. https://atlas.nve.no/Html5Viewer/index.html?viewer=nveatlas#, last access: 23 September April 2020.

Oppikofer, T., Böhme, M., Nicolet, P., Penna, I.M., and Hermanns, R.L.: Metodikk for konsekvensanalyse av fjellskred, Geol. Surv. Norw., Trondheim, Norway, NGU report 2016.047, 67 pp., 2016a (in Norwegian).

Oppikofer, T., Hermanns, R.L., Sandøy, G., Böhme, M., Jaboyedoff, M., Horton, P., Roberts, N.J., and Fuchs, H.: Quantification of casualties from potential rock-slope failures in Norway, in: Landslides and Engineered Slopes. Experience, Theory and Practice, edited by: Aversa, S., Cascini, L., Picarelli, L., and Scavia, C., Associazione Geotecnica Italiana, Rome, Italy, 1537–1544, 2016b.

Oppikofer, T., Hermanns, R.L., Roberts, N.J., and Böhme, M.: SPLASH: semi-empirical prediction of landslide-generated displacement wave run-up heights, in: Subaqueous Mass Movements and Their Consequences: Assessing Geohazards, Environmental Implications and Economic Significance of Subaqueous Landslides, edited by: Lintern, D.G., Mosher, D.C., Moscardelli, L.G., Bobrowsky, P.T., Campbell, C., Chaytor, J.D., Clague, J.J., Georgiopoulou, A., Lajeunesse, P., Normandeau, A., Piper, D.J.W., Scherwath, M., Stacey, C., Turmel, D., Geological Society of London Special Publications, 477, 353–366, https://doi.org/10.1144/SP477.1, 2019.

Plaza, G., Zevallos, O., Cadier, E.: La Josefina Landslide Dam and Its Catastrophic Breaching in the Andean Region of Ecuador, in: Natural and Artificial Rockslide Dams, edited by: Evans, S.G., Hermanns, R.L., Strom, A., Scarascia-Mugnozza, G., Lecture Notes in Earth Sciences, vol. 133, Springer, Berlin, Heidelberg, Germany, 389–406, 2011.

Scheidegger, A.E.: On the prediction of the reach and velocity of catastrophic landslides. Rock Mech., 5, 231–236, (1973.

Schleier, M., Hermanns, R.L., Rohn, J., and Gosse, J.C.: Diagnostic characteristics and paleodynamics of supraglacial rock avalanches, Innerdalen, Western Norway. Geomorphology, 245, 23-39, http://dx.doi.org/10.1016/j.geomorph.2015.04.033, 2015.

Schleier, M., Hermanns, R.L., Gosse, J.C., Oppikofer, T., Rohn, J., and Tønnesen, J.F.: Subaqueous rock-avalanche deposits exposed by post-glacial isostatic rebound, Innfjorddalen, Western Norway. Geomorphology, 289, 117-133, https://doi.org/10.1016/j.geomorph.2016.08.024, 2017.

Sosio, R., Crosta, G.B., and Hungr, O.: Complete dynamic modeling calibration for the Thurwieser rock avalanche (Italian Central Alps). Engineering Geology, 100, 11-26, https://doi.org/10.1016/j.enggeo.2008.02.012, 2008.

Tacconi Stefanelli, C., Catani, F., and Casagli, N.: Geomorphological investigations on landslide dams. Geoenviron. Disasters, 2, 21, https://doi.org/10.1186/s40677-015-0030-9, 2015.

Tacconi Stefanelli, C., Segoni, S., Casagli, N., and Catani, F.: Geomorphological analysis for landslide dams, in: Landslides and Engineered Slopes. Experience, Theory and Practice, edited by: Aversa, S., Cascini, L., Picarelli, L., and Scavia, C., Associazione Geotecnica Italiana, Rome, Italy, 1883–1887, 2016.

Tacconi Stefanelli, C., Vilímek, V., Emmer, A., and Catani, F.: Morphological analysis and features of the landslide dams in the Cordillera Blanca, Peru. Landslides, 15, 507–521, https://doi.org/10.1007/s10346-017-0888-6, 2018.

Tochnog Professional: Tochnolog Professional Finite Element Analysis, http://www.tochnogprofessional.nl, 2020.

Weidinger, J.T.: Stability and life span of landslide dams in the Himalayas (India, Nepal) and the Qin Ling Mountains (China), in: Natural and Artificial Rockslide Dams, edited by: Evans, S.G., Hermanns, R.L., Strom, A., Scarascia-Mugnozza, G., Lecture Notes in Earth Sciences, vol. 133, Springer, Berlin, Heidelberg, Germany, 243–277, 2011.

581   **Figures**
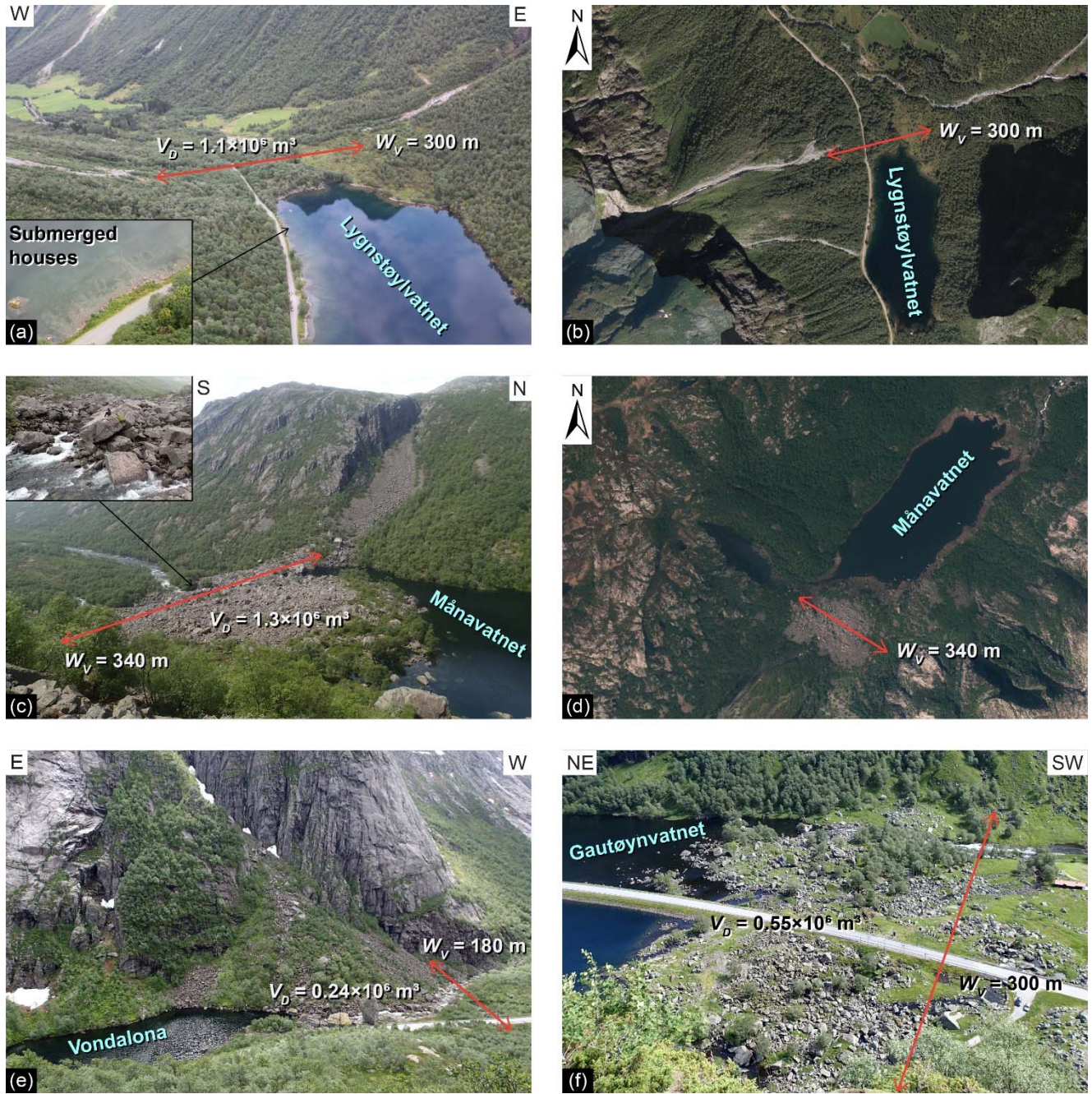
582

583   **Figure 1: Photographs of RSF dams in southwestern Norway with dam volume V_D and valley width W_V: (a) the lake**
584   **Lygnstøylvatnet was created by the 1908 rock avalanche from the mountain Keipen in the West. The rock avalanche went over**
585   **an existing debris cone and abutted against a debris cone on the opposite valley side leading to a type IIb dam that is intact (dam**
586   **classification by Hermanns et al. 2011b). The remains of submerged houses are visible in Lygnstøylvatent (inset); (b) orthophoto**
587   **of Lygnstøylvatnet (Norwegian Mapping Authority, 2020b); (c) the lake Månavatnet was dammed by a 1.3×10^6 m³ rock**
588   **avalanche coming from the Northwest. The type IIa dam is stable until now with drainage through the rock avalanche deposits**
589   **(inset); (d) orthophoto of Månavatnet (Norwegian Mapping Authority, 2020b); (e) the lake Vondalona was created by a small rock**
590   **avalanche in the narrow valley and the type IIc dam is partly eroded by the river; (f) the lake Gautøynvatnet is located only 3.7 km**
591   **downstream of lake Vondalona and was dammed by a 0.55×10^6 m³ rock avalanche that completely crossed the valley. The type**
592   **IIa dam is partly eroded by the river.**

593

594 **Figure 2: Inventory maps of dams from rock slope failures and unstable rock slopes in Norway: (a) dam inventory of southwestern**
595 **Norway classified according to dam stability (modified from Jakobsen, 2015) underlain by the landform classification by**
596 **Etzelmüller et al. (2007); (b) overview map of unstable rock slopes in Norway (per December 2019) that may lead to a rockslide**
597 **dam in case of catastrophic failure (data from NGU, 2020), along with the location of existing dams in northern Norway used as**
598 **validation dataset; (c) zoom on the rockslide dam clusters in Rogaland County. Rock avalanche dams discussed in the text are (in**
599 **blue font): Ke = Keipen, Li = Lintuvatnet, Mv = Månavatnet, Vo = Vondalona, Gv = Gautøynvatnet, La = Langfjordura, Gr =**
600 **Grøtnesura, Kv = Kvarteurda, St = Steinura. Unstable rock slopes mentioned in the text are (in red font): Ga = Gamanjunni, Iv**
601 **=Ivasnasen, Kl = Klingråket, Ma = Mannen, Sv = Svarttinden.**

(a) Plan view

(b) Across-valley profile

(c) Along-valley profile
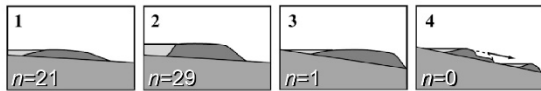
Figure 3: Morphologic classification of landslide dams (modified from Hermanns et al., 2011b) with count of landslide dams in southwestern Norway: (a) in plan view, dams formed by a landslide completely crossing the valley (Type IIa) are most common, followed by partial damming of the valley (Type IIc) and landslide dams having multiple lakes (Type IIIa); (b) in across-valley profile, most dams are symmetrical deposits in a symmetrical valley (Type i) or asymmetrical with thickest deposits in the distal part (Type ii); (c) in along-valley profile, dams with low thickness and gentle slopes (Type 1) and dams with high thickness and steep slope (Type 2) are most abundant.
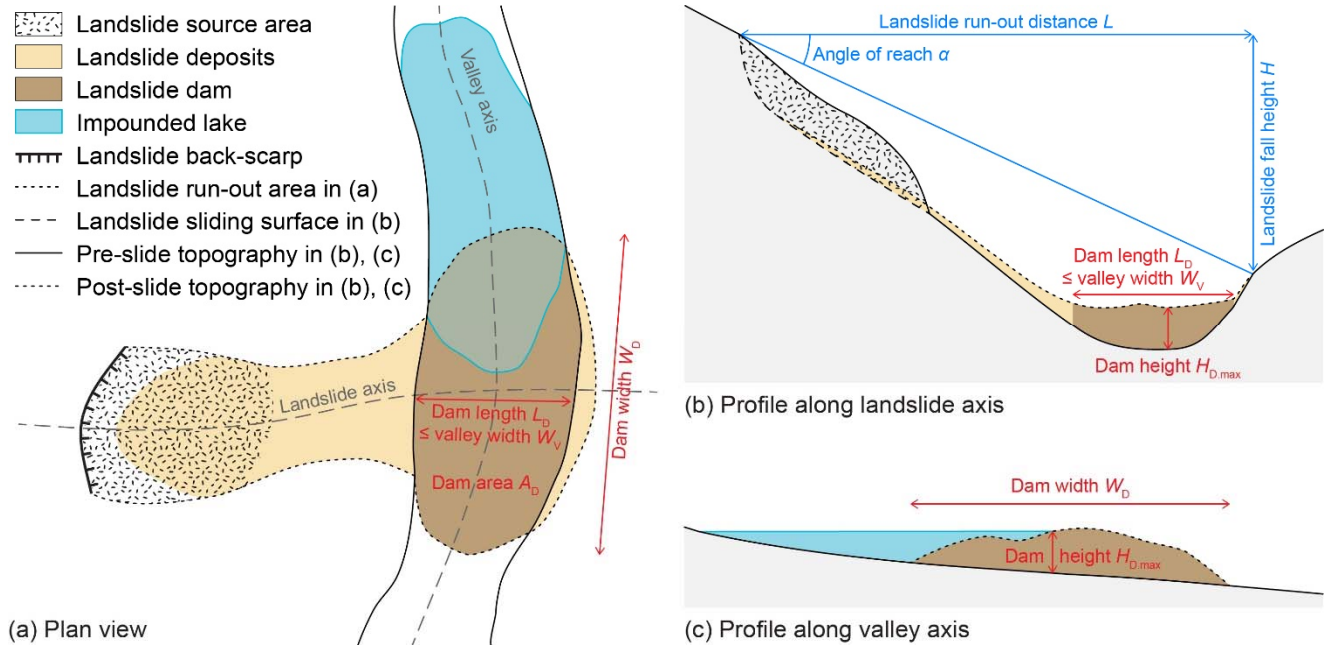
Figure 4: Sketches of a landslide dam with the measured dimensions (adapted from Toccani Stefanelli et al., 2018): (a) plan view for measuring dam area A_D, dam width W_D, dam length L_D and valley width W_V ($L_D = W_V$ in case of complete damming of valley, $L_D < W_V$ in case of partial damming of valley); (b) across-valley profile for measuring valley width W_V, dam length L_D and estimating maximum dam height $H_{D.max}$, along with landslide fall height H, landslide run-out distance L and angle of reach α; (c) along-valley profile for measuring dam width W_D and estimating maximum dam height $H_{D.max}$. The pre-landslide topography is estimated on both profiles by considering the local valley morphology.

616
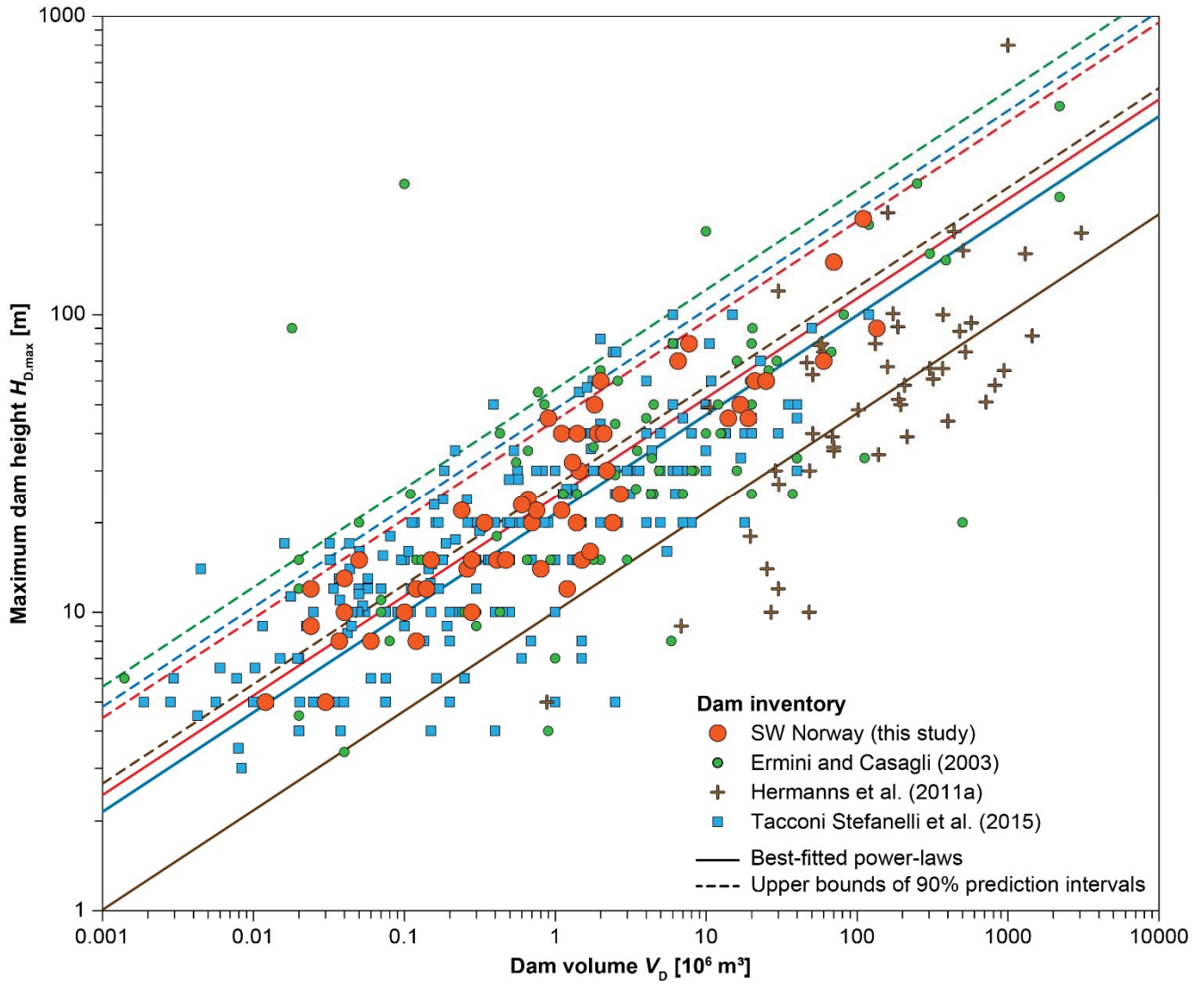
617 **Figure 5: Relationship between maximum dam height $H_{D.max}$ and dam volume V_D (in 10^6 m³) for RSF dams in southwestern**

618 **Norway (data from Jakobsen, 2015), compared to datasets from Ermini & Casagli (2003), Hermanns et al. (2011a) and Tacconi**

619 **Stefanelli et al. (2015). The maximum dam heights increase with dam volume according to power-law distributions as in Eq. (2)**

620 **with scale factors as in Table 2 (with colours matching the point symbols).**

621
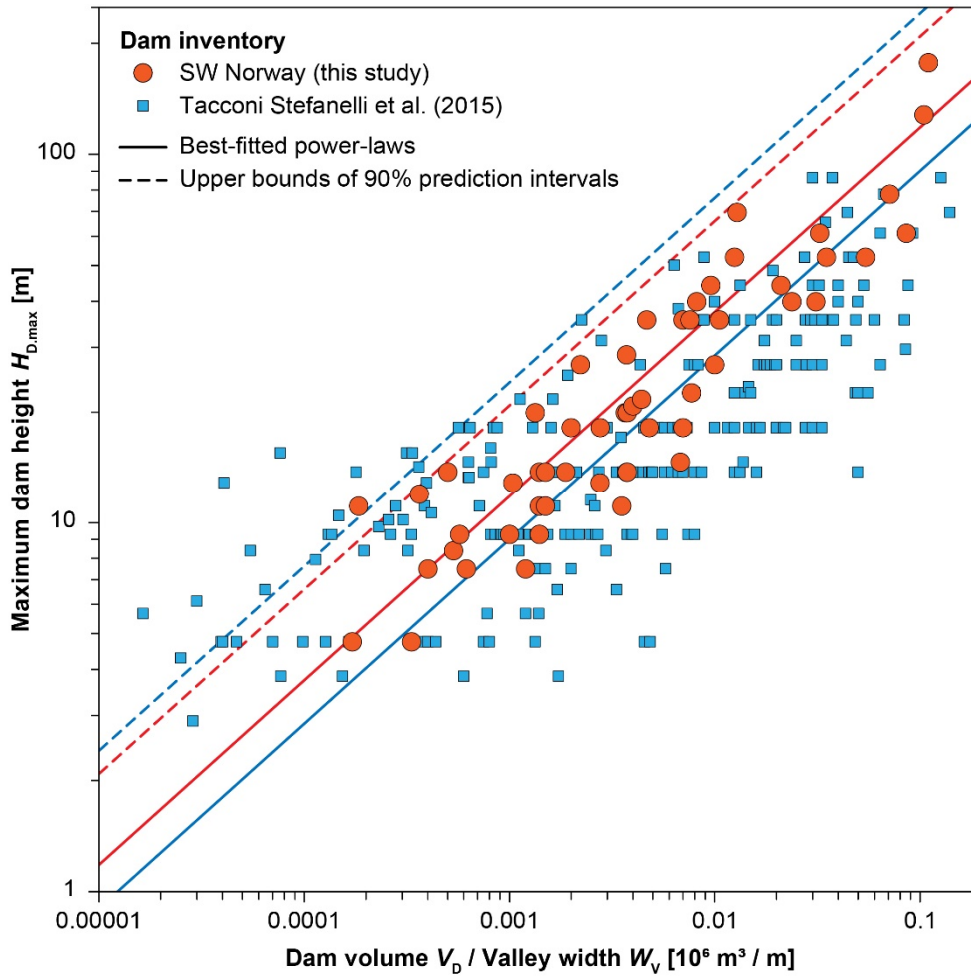
622 **Figure 6: Relationship between maximum dam height $H_{D.max}$ and the ratio between dam volume V_D (in 10^6 m³) and valley width**

623 **W_V (in m) for RSF dams in southwestern Norway (data from Jakobsen, 2015), compared to the dataset from Tacconi Stefanelli et**

624 **al. (2015). $H_{D.max}$ increases with V_D/W_V according to power-law distributions as in Eq. (3) with scale factors as in Table 2 (with**

625 **colours matching the point symbols).**

626

Figure 7: Linear relationship between maximum dam height $H_{D.max}$ and mean dam height $H_{D.mean}$ – computed as the ratio of dam

volume V_D over dam area A_D – for RSF dams in southwestern Norway (data from Jakobsen, 2015), compared to the dataset from

Tacconi Stefanelli et al. (2015). Linear regressions as in Eq. (4) with scale factors as in Table 2 and the upper bounds of the 90%

prediction intervals are shown with colours matching the point symbols.

631
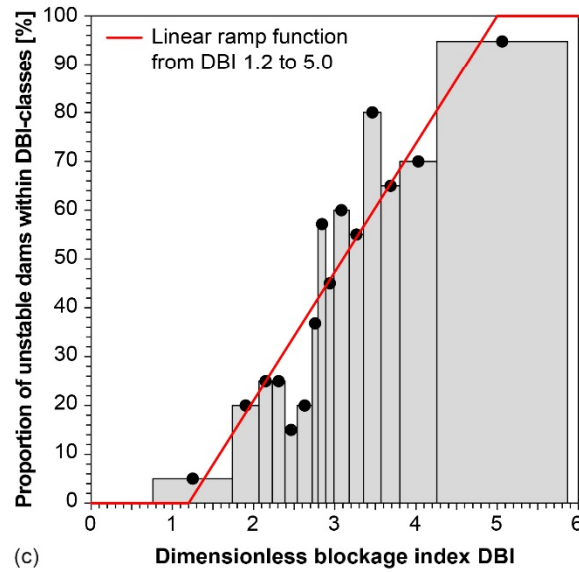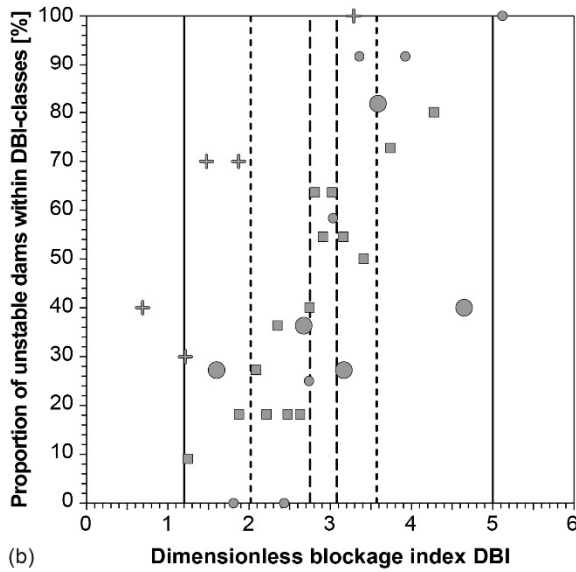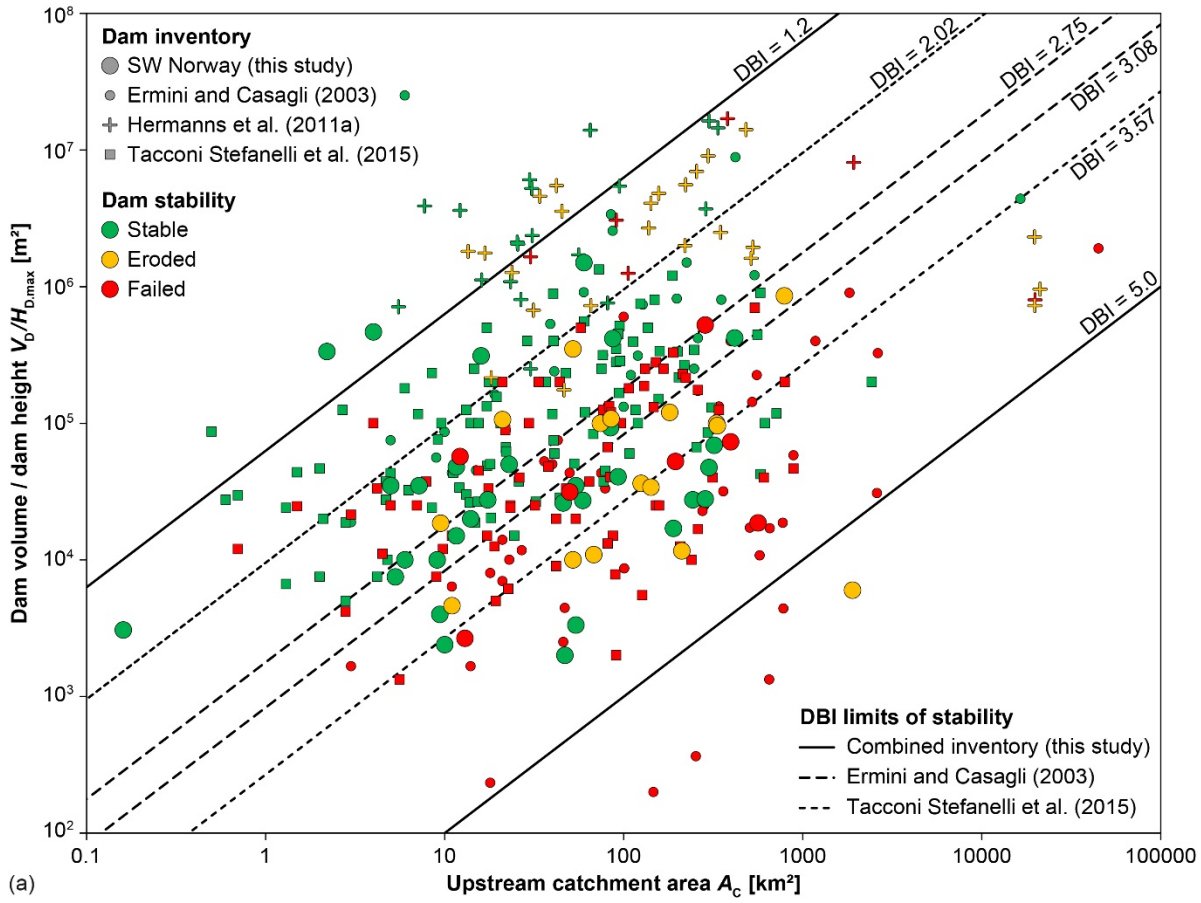
632 **Figure 8: The dimensionless blockage index (DBI) for RSF dams in southwestern Norway: (a) the ratio dam volume V_D / maximum**

633 **dam height $H_{D.max}$ is plotted against the upstream catchment area A_C for stable and unstable dams, along with the lower and upper**

634 **DBI-limits from Ermini and Casagli (2003), Tacconi Stefanelli et al. (2015) and this study separating the stability domain from**

635 **the instability domain with a transition zone in between; (b) proportions of unstable dams for bins of DBI-values (each containing**

636 **10-12 landslide dams) for different inventories along with their DBI-limits (see legend in (a)); (c) for the combined inventory of**

637 **landslide dams (Ermini and Casagli, 2003, Tacconi Stefanelli et al., 2015 and our dataset) the proportion of unstable dams**

638 **increases with DBI. A linear function is used between DBI-values of 1.2 and 5.0 to assess the likelihood of a dam failure p_f.**
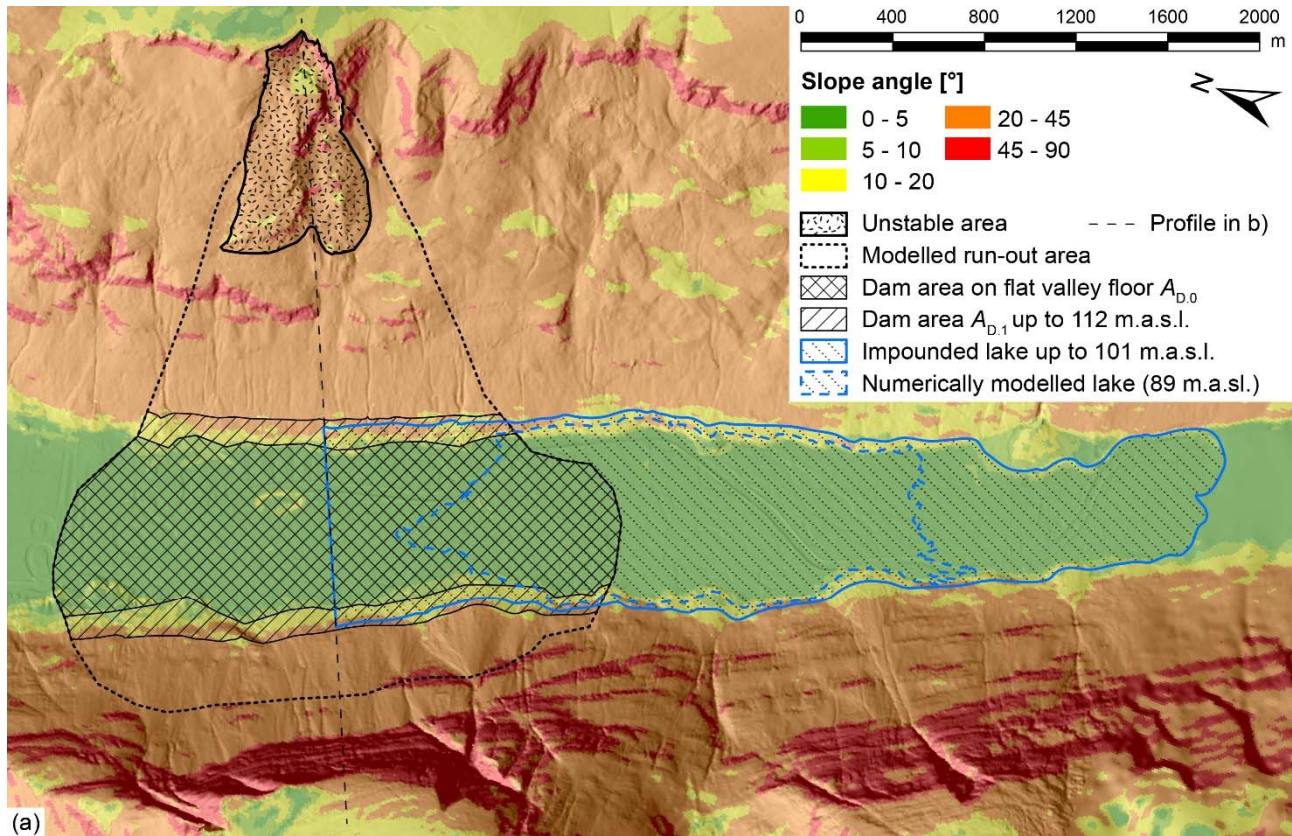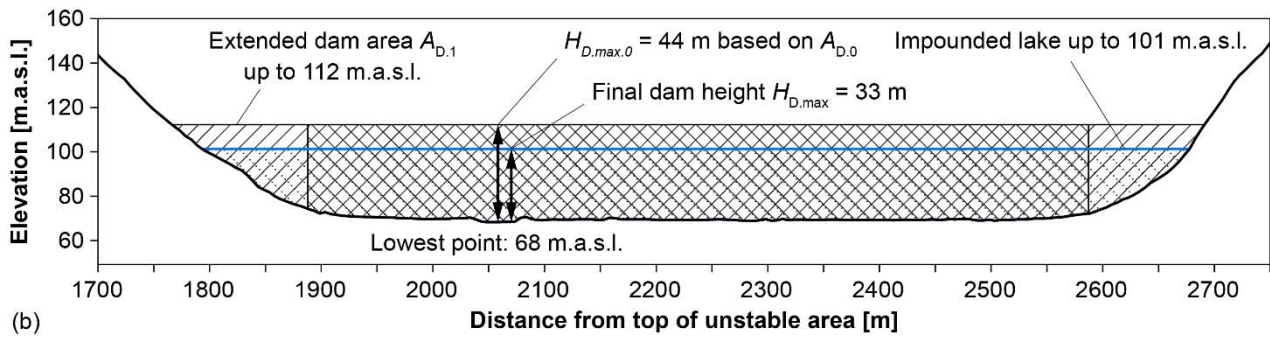
Figure 9: Iterative procedure to estimate the maximum dam height $H_{D.max}$ using the modelled run-out area to estimate the dam area A_D. The example shown is the 21×10^6 m³ rockslide of Gamanjunni 3 in Northern Norway (Böhme et al., 2016), which might lead to a 33 m high landslide dam using Eq. (4) with the iterative procedure to assess the possible dam area A_D.

Tables

Table 1 Descriptive statistics of RSF dam dimensions in southwestern Norway and lognormal distributions matching the cumulative frequency distributions of the dimensions.

	Valley width W_V [m]	Dam length L_D [m]	Dam width W_D [m]	Dam area A_D [m²]	Maximum dam height $H_{D.max}$ [m]	Mean dam height $H_{D.mean}$ [m]	Dam volume V_D [m³]
Basic statistics							
Average	310	300	520	220 000	34	20	9 600 000
Median	200	200	330	53 000	21	12	1 000 000
Min	45	42	45	5000	5	2	12 000
Max	1900	1600	2800	2 700 000	210	113	135 000 000
Lognormal distribution							
Expected value (mean)	5.41	5.34	5.88	11.09	3.16	2.60	13.69
Standard deviation	0.811	0.846	0.863	1.533	0.823	0.908	2.283
r^2	0.967	0.980	0.917	0.961	0.953	0.959	0.951

Table 2 Fitting parameters of the semi-empirical relations for different studies.

Study	Eq. (2) (exponent ⅓)			Eq. (3) (exponent ½)			Eq. (4) (exponent 1)		
	Scale factor	r^2	ρ_{95}	Scale factor	r^2	ρ_{95}	Scale factor	r^2	ρ_{95}
Ermini & Casagli (2003)	21.6	0.782	2.62						
Hermanns et al. (2011a)	10.1	0.351	2.65						
Tacconi Stefanelli et al. (2015)	21.5	0.537	2.25	285	0.583	2.67	1.35	0.652	1.84
This study (all dams, n=54)	24.5	0.735	1.81	374	0.787	1.76	1.75	0.957	1.48
This study (Type i dams, n=24)	22.6	0.707	1.76	347	0.808	1.56	1.74	0.969	1.36
This study (Type ii dams, n=19)	27.0	0.811	1.76	395	0.838	1.77	1.65	0.977	1.45
This study (Type iv dams, n=6)	29.3	0.924	2.05	432	0.748	2.48	1.93	0.847	1.92
This study (Type 1 dams, n=21)	21.1	0.905	1.63	361	0.899	1.71	1.85	0.919	1.52
This study (Type 2 dams, n=29)	27.6	0.795	1.80	382	0.783	1.76	1.67	0.964	1.43

650 **Table 3 Dam characteristics for past rock avalanche dams or modelled potential future rock avalanche dams in comparison with predicted dam characteristics from semi-empirical relationships. Predicted DBI-values and probability of dam failure p_f are indicated for predicted $H_{D.max}$ using Eq. (4). The predicted $H_{D.max}$-, DBI- and p_f-values are shown for the best-fitted equation and in parentheses the values obtained from the upper bound of the 90% prediction interval (ρ_{95}). The best match between measured/modelled and empirically predicted maximum dam heights is highlighted in grey. For future landslide dams the dam volume V_D equals the landslide volume V_S times a bulking factor of 1.25 (Hungr and Evans, 2004).**

Site	Dam volume V_D [10^6 m³]	Valley width W_V [m]	Dam area A_D [km²]	Catchment area A_C [km²]	Measured/modelled dam characteristics			Empirically predicted dam characteristics				
					Maximum dam height $H_{D.max}$ [m]	Dimension-less blockage index DBI [-]	Probability of failure p_f [%]	Maximum dam height $H_{D.max}$			Dimension-less blockage index DBI [-]	Probability of failure p_f [%]
								$f(V_D)$ (Eq. (2)) [m]	$f(V_D, W_V)$ (Eq. (3)) [m]	$f(V_D, A_D)$ (Eq. (4)) [m]		
Past rock avalanche dams in Northern Norway												
Grøtnesura	14.5	800	0.58	18	50	1.79	15%	60 (108)	50 (89)	44 (65)	1.73 (1.90)	14% (18%)
Kvarteurda	16.8	620	0.44	29	60	2.02	21%	63 (114)	62 (109)	67 (99)	2.06 (2.23)	23% (27%)
Langfjordura	15	670	0.58	5	40	1.08	0%	60 (109)	56 (99)	45 (67)	1.14 (1.31)	0% (3%)
Steinura	12	550	0.46	21	40	1.85	17%	56 (102)	55 (97)	46 (67)	1.90 (2.07)	18% (23%)
Potential future rock avalanche dams												
Gamanjunni	26	925	2.05	150	18	2.01	21%	73 (122)	63 (99)	22 (33)	2.11 (2.28)	24% (28%)
Ivasnasen	2.8	220	0.31	1670	11.6	3.85	70%	34 (58)	42 (66)	16 (23)	3.98 (4.15)	73% (78%)
Klingråket	0.29	260	0.093	2264	7.8	4.79	94%	16 (27)	12 (20)	5 (8)	4.63 (4.80)	90% (95%)
Mannen B	24	900	2.23	1170	17	2.93	45%	70 (118)	60 (95)	18 (27)	2.96 (3.13)	46% (51%)
Mannen C	3.6	900	0.77	1170	7	3.35	57%	38 (63)	24 (37)	8 (12)	3.43 (3.60)	59% (63%)
Svarttinden	3.7	650	0.85	1137	6.5	3.30	55%	38 (64)	28 (44)	8 (11)	3.37 (3.54)	57% (62%)